Instabilities and routes to turbulence in rotating disc boundary layers and cavities

D. Martinand, E. Serre, B. Viaud

PHILOSOPHICAL TRANSACTIONS A

rsta.royalsocietypublishing.org

Research

Article submitted to journal

Subject Areas:
xxxxx, xxxxx, xxxx

Keywords:
xxxx, xxxx, xxxx

Author for correspondence:
Eric Serre
e-mail: eric.serre@univ-amu.fr

Instabilities and routes to turbulence in rotating disk boundary layers and cavities

D. Martinand[1], E. Serre[1] and B. Viaud[2]

[1] Aix-Marseille Univ., CNRS, Centrale Marseille, M2P2, Marseille, France

[2] CReA - École de l'air et de l'espace Salon-de-Provence, France

Studied for more than a century, first in the field of geophysics, flows over rotating disks present a great diversity of complex instability behaviours, that are not yet fully understood. While the primary instabilities are now well characterised experimentally, theoretically and numerically, their role in the transition mechanisms to turbulence remains an open question that still challenges the scientific community. This article brings together the main results of the literature related to the instabilities over rotating disks, but also in the connected problem of rotating cavities and reviews the main scenarios currently assumed to describe the flow breakdown to turbulence. A particular focus is made on more recent studies of generic flows in rotating cavities bounded by two coaxial rotating disks, that occur in many industrial systems, the performances of which and their improvement being linked to a better understanding of these mechanisms.

1. Introduction

Since Taylor's seminal article in 1923 [1], the centenary of which is celebrated in this special issue, it is demonstrated that in a viscous fluid between two coaxial rotating cylinders (Taylor–Couette flow), the curvature of the flow, or, equivalently, the centrifugal force, is a source of instability, potentially leading to vortices stacked in the annular gap. In this paper, we are rather interested in the stability of flows in rotating disk cavities, which can be seen as flattened Taylor–Couette set-ups, of aspect ratios $\Gamma = h/\Delta R \ll 1$, with h the height of the cavity and $\Delta R = R_{out} - R_{in}$ the width of the annular gap. The boundary layers on the endwall disks, of marginal role in the stability of the Taylor–Couette flow (see [2,3] for an account of these effects), then become dominant.

THE ROYAL SOCIETY PUBLISHING

These rotating disk cavities are present in a wide variety of industrial systems, such as electronic products, with the hard disk drives, the automotive industry, with the disk brakes, or turbo-machinery, with the compressor and turbine disks, to cite but a few. An overview of the variety of configurations and applications may be found in the books of Owen & Rogers [4,5]. This review more specifically focuses on the rotor-stator flows, arising between a rotating disk and a stationary one, and the forced, source flows between two co-rotating disks, which are the two main configurations of rotating cavities investigated theoretically, numerically and experimentally in the literature, as canonical models of more complex industrial systems [4–7] and geophysical flows [8].

A distinctive feature of these configurations is the coexistence of adjacent and coupled flow regions that radically differ in terms of boundary layer thickness scales and flow stability properties. The present review limits its scope to flows between two disks separated by a height h where the thin viscous boundary layers over the disks are kept apart by a large quasi non-viscous, geostrophic, core region in solid-body rotation. This amounts to flows at large Reynolds numbers ($Re_h = (h/\delta)^2 \gg 1$), the boundary layers thicknesses scaling with the viscous characteristic length $\delta = (\nu/\Omega)^{1/2}$ [9], with ν the kinematic viscosity of the fluid and Ω a characteristic angular velocity (more details will be provided in Sec. 3). Torsional Couette-type flows in rotor-stator cavities at small Re_h are not addressed here (see [10,11] for details on these flows). In the present configurations, the stability properties of the flow are therefore dominated by the stability properties of the boundary layers over each disk. The instability mechanisms in these boundary layers are akin to those of single disk flows. The radial confinement and the coupling between the different flow regions in the cavity, however, may lead to specific stability properties and different transition mechanisms to turbulence.

Single disk flows have been the subject of fundamental interest, as prototype flows for three-dimensional boundary layers, and as a basic model in geophysics and astrophysics to investigate the dynamics of the atmospheric boundary layers and of the wind-driven surface layers of the ocean. Unlike the flow over a swept wing, however, the Navier–Stokes equations admit here exact similarity solutions, as demonstrated by von Kármán [12] and summarized in Sec. 2, making this flow the archetype of the three-dimensional boundary layers for all investigations. This interest has led to numerous publications in the literature since the fifties (see [13] for a review). When the disk rotating in an otherwise still fluid is infinite, the base flow is parallel (independent on the radial position), with a laminar velocity profile presenting one or several inflection point(s), and, thus, susceptible to lead to an inviscid crossflow instability. Among the first visualizations of instability patterns in the form of spiral arms reported in the literature are certainly those of Smith [14] and Gregory, Stuart & Walker [15]. Since then, numerous theoretical [16] and experimental [17–20] works have categorized these instabilities into type I (crossflow instability) and type II (combined effects of Coriolis and viscous forces), and have investigated their properties depending on the flow conditions (see Sec. 4). The interest for this flow was largely renewed by the works of Lingwood [21–24], which first demonstrated the type I, crossflow, instabilities transiting from convective to absolute at a Reynolds number slightly below its value characterizing the onset of turbulence in experiments, suggesting a direct route to turbulence driven by absolute instabilities. This led to a new string of theoretical, experimental and numerical papers investigating such a scenario of transition, and the impact of several flow features on it, such as the presence of roughness on the disk [25,26], non-parallel effects [27–29] or edge effects in systems with finite radius [30–33] (see Sec. 5).

These results can be extended to flows between two coaxial disks, when $Re_h \gg 1$. Batchelor [34,35] generalized the analyses of von Kármán to two-parameter families of solutions having a mathematical structure similar to that of von Kármán's. It should nonetheless be kept in mind that the von Kármán equations are non-linear and the uniqueness of their solutions remains an open question in infinite systems [36]. For the flow between two co-rotating infinite disks, he

argued that at high Reynolds number, the fluid between the disk would rotate with a constant angular velocity (the so-called geostrophic velocity) and that boundary layers would form upon both disks (see Sec. 2). Itoh [37] and Serre *et al.* [38] investigated the linear stability of Batchelor's solution between a rotating disk and a stationary one. As for the single disk rotating in a still fluid or stationary in a rotating fluid, the boundary layer on the rotating disk was found to be substantially more stable than the one on the stationary disk. The results of Serre *et al.* suggested that on the rotating disk, the linear threshold of instability as well as the convective/absolute transition in the two-disk configuration were close to the results obtained for the single disk boundary layer, although a lack of data in the literature prevented an accurate extrapolation of the results to the corresponding Rossby number, as measured from the geostrophic velocity at mid-height.

Instabilities in finite-size cavities may behave differently. Even if the instability mechanisms in the two separated boundary layers are similar to those of single disks, works in the literature have displayed specific features of the flow structure and stability, justifying dedicated studies [6,7]. The confinement in the radial direction in the rotor-stator cavity and the conservation of the mass flow rate in the co-rotating cavity with throughflow introduce a spatial inhomogeneity in the flow, which leads to non-parallel boundary layers and to stability properties varying with the radius. Thus, the reference to similarity solutions obtained at constant Rossby number, can only have a local meaning. Moreover, in rotor-stator cavities, the confinement restricts this local description to a region of finite radial extent, remote from the edge and the axis [39–42]. As a consequence, the stability of such flows must be addressed within the framework of global stability analysis (see examples in [43,44]). When the cavity is closed by a shroud and possibly a shaft, as in annular rotor-stator configurations, or when the flow exhibits an entry zone upstream the boundary layers form, as in the open cavity with radial througflow, the stability properties are also further impacted. Indeed, other instability mechanisms can occur within the vertical boundary layers [38,44–46] or in the entry zone [47] which can introduce disturbances in the flow. All this modifies the scenarios of transition to turbulence in the rotating cavities with respect to that on the single disk flow, as discussed in Sec. 5.

The single disk configurations and the rotating disks cavities considered in this review are described in Sec. 2, and the analytical expressions of the base flows in the different configurations of infinite radial extension are briefly addressed. The dimensionless parameters characterising the flows and how they relates in the different configurations are introduced in Sec. 3. The main theoretical, numerical and experimental results from the literature concerning the boundary layer instabilities of rotating disks are then discussed and summarised in Sec. 4. Finally, the main scenarios currently assumed to describe the flow breakdown to turbulence are introduced in Sec. 5.

2. Geometry and base flows, from single disks to the rotating cavities

A wide range of geometrical configurations, with one or two rotating disks, have been investigated in the literature, to perform fundamental research on rotating flows properties or to optimize complex technological or engineering systems. In engineering applications, the fluid usually flows inside rotating disks cavities that mimic, more or less realistically, parts of more complex devices. A typical geometrical feature is the wheel-space cavity formed between plain rotating disks separated by a height h. A wide range of set-ups are possible [4,5,48], with various fluids and physics, disks of various shapes, natures, rotation rates and related boundary conditions. Geometrically, these set-ups include cylindrical (with a shroud at the outer radius R_{out}) or annular (with the addition of a shaft at the inner radius R_{in}), cavities. Moreover, open cavities presenting net superimposed axial or radial through-flows are also

considered. The exhaustive review of all configurations would be strenuous and we only consider here incompressible Newtonian fluids and planar impermeable disks with no-slip boundary conditions, excluding peculiar configurations with compliant wall, porous wall, heated wall or others. This review then addresses the three following configurations:

- single disks, rotating at rate Ω_d in a still fluid, or stationary in a fluid rotating at rate Ω_f,
- open cavities with radial through-flow between two disks co-rotating at rate Ω_d,
- closed cavities between a rotor rotating at rate Ω_d and a stator,

with a specific and original focus on the two cavity flows. Sketches of these configurations and their theoretical base flows are shown in Figures 1,2 and 3. With respect to the fundamental studies of the flows dynamics, single disks and rotating cavities configurations both have advantages and drawbacks. On the one hand, fundamental investigations to characterize flow properties in laminar and turbulent regimes remain largely based on finite-radius single-disk experimental set-ups. This configuration allows to avoid confinement-related issues (even if some edge-related questions have been recently raised in the literature) and facilitate direct comparisons with theoretical studies based on similitude solutions and stability analysis valid in infinite systems. Experimentally, the single disk configuration is also well suited for optical velocimetry techniques. On the other hand, Direct Numerical Simulations are easier in confined rotating cavity flows than in unconfined single disk flows. These two cavity configurations allow to connect the single disk flow and more complex geometries related to industrial devices. Thus, they bridge the gap between theory and engineering to provide useful flow characteristics at the design stage of rotating machines for their optimisation. First, the laminar and steady flows in rotating cavities are closely related to the ones observed and computed over a single disk. The analytical approaches used to get further insight to the laminar steady flows in these configurations, in systems of infinite radial extension, are build on the early works of von Kármán [12] and Ekman [49], and are briefly summarized hereinafter.

(a) From von Kármán and Bödewadt boundary layers to rotor-stator flows

In the approach of von Kármán [12], the canonical laminar flow over a rotating disk of infinite radius amounts to seek a steady axisymmetric flow by separation of variables, with imposed rotation of the disk and solid rotation of the fluid at infinity above it. Using cylindrical coordinates (r, θ, z), with z the direction of the rotation axis, the radial, azimuthal and axial components of the velocity read:

$$u = \widetilde{\Omega} r F\left(\frac{z}{\delta}\right), \quad v = \widetilde{\Omega} r G\left(\frac{z}{\delta}\right) \quad \text{and} \quad w = \widetilde{\Omega}\delta H\left(\frac{z}{\delta}\right), \tag{2.1}$$

respectively, where $\widetilde{\Omega}$ is a characteristic rotation rate and δ a characteristic boundary layer thickness.

Injecting expressions (2.1) in the incompressible Navier–Stokes and continuity equations expressed in the inertial frame turn them into a system of non-linear ordinary differential equations satisfied by the axial shape functions of the velocity profile:

$$\begin{gathered} H' + 2F = 0 \\ F''' - \frac{\delta^2\widetilde{\Omega}}{\nu}\left[2F'F + F'H' + HF'' + 2GG'\right] = 0 \\ G'' - \frac{\delta^2\widetilde{\Omega}}{\nu}\left[2FG + G'H\right] = 0, \end{gathered} \tag{2.2}$$

together with boundary conditions at the disk and at infinity. This system of equations is usually solved numerically. Two cases have gained specific attention, at least for historical reasons.

The von Kármán flow [12] assumes a disk rotating at angular velocity Ω_d with no solid rotation of the fluid at infinity ($\Omega_f = 0$), which corresponds to $\widetilde{\Omega} = \Omega_d$, $\delta = \sqrt{\nu/\Omega_d}$ and related boundary

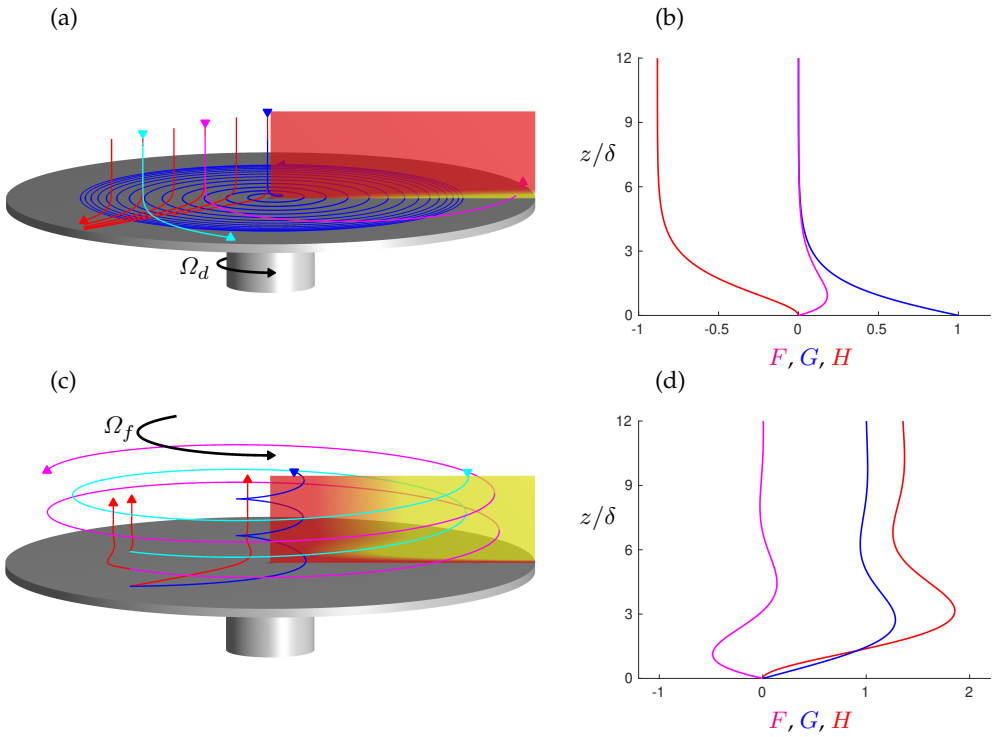

Figure 1: Similarity solutions in a single disk configuration. (a) and (b): Von Kármán solution over a rotating disk and (c) and (d): Bödewadt solution over a stationary disk, both in the inertial frame. The meridional planforms in (a) and (c) show the azimuthal component of the velocity. A few streamlines in the whole space are depicted by the blue, magenta and cyan curves and the corresponding streamlines restricted to a meridional plan by red ones. (b) and (d): Axial shape functions F (magenta), G (blue) and H (red) of the velocity profile, as functions of z/δ.

conditions:

$$\begin{array}{l} F(0)=0,\ G(0)=1 \text{ and } H(0)=0 \\ \lim_\infty F=0,\ \lim_\infty G=0 \text{ and } \lim_\infty G'=0. \end{array} \tag{2.3}$$

As shown by the streamlines in panel (a) and axial shape functions in panel (b) of figure 1, beside its rotation, the fluid is centrifuged along the disk and this radial outflow is fed by the fluid being pumped from above. Despite F, G and H being of similar orders of magnitude, the prefactors in expressions (2.1) impose that for radii $r \gg \delta$ and in the vicinity of the disk, the axial flow is small compared to the radial and azimuthal components.

The Bödewadt flow [50] assumes a stationary disk ($\Omega_d = 0$) with a fluid in solid-body rotation Ω_f at infinity, which corresponds to $\widetilde{\Omega} = \Omega_f$, $\delta = \sqrt{\nu/\Omega_f}$ and related boundary conditions:

$$\begin{array}{l} F(0)=0,\ G(0)=0 \text{ and } H(0)=0 \\ \lim_\infty F=0,\ \lim_\infty G=1 \text{ and } \lim_\infty G'=0. \end{array} \tag{2.4}$$

In a fashion opposite to the von Kármán case, the fluid is now ejected above the disk, inducing a radial inflow near the disk, as shown by the streamlines in panel (c) and axial shape functions in panel (d) of figure 1. Beside this overall upward whirlwind of fluid (blue, cyan and magenta streamlines), the corresponding trajectories in a meridional plane (red streamlines) are noticeably more intricate than in the von Kármán case, mixing centrifugal and centripetal movements. Indeed, despite being obtained from the same equations and similar boundary conditions, it can be seen on figure 1(d) that the velocity profile presents several inflexion points and for an identical

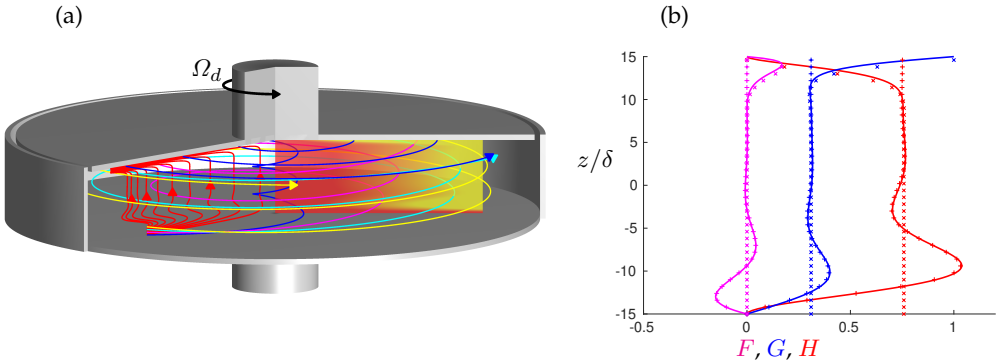

Figure 2: Rotor-stator flow in the inertial frame. (a) The meridional plan shows the azimuthal component of the velocity. Streamlines in the whole space (blue, magenta, cyan and yellow curves) and same streamlines restricted to a meridional plan (red curves). (b) Comparison between the Batchelor solution (solid curves) and the respective von Kármán (on the rotor above, marked by x symbols) and Bödewadt (on the stator below, marked by crosses) solutions. Axial shape functions F (magenta), G (blue) and H (red) of the velocity profile, as functions of z/δ.

viscous length δ, the Bödewadt layer extends substantially further away from the disk than the von Kármán layer.

Building on the approach by von Kármán, Batchelor [34] considered a cavity of height h, confined between two disks in differential rotation. For a configuration with a rotor above and a stator below, as addressed in the forthcoming, the laminar flow in an axially confined system of infinite radial extension can be obtained from the von Kármán equations (2.2), together with the boundary conditions

$$\begin{aligned} &F(0)=0,\ G(0)=0 \text{ and } H(0)=0 \\ &F(h/\delta)=0,\ G(h/\delta)=1 \text{ and } H(h/\delta)=0. \end{aligned} \tag{2.5}$$

In this configuration, $\widetilde{\Omega}=\Omega_d$ and $\delta=\sqrt{\nu/\Omega_d}$. As shown in figure 2(b), the flow developing in this rotor-stator cavity develops two boundary layers that can be seen as a von Kármán flow near the rotor matched to a Bödewadt one near the stator. This mating is achieved by setting the prescribed rotation rates far from the disks in both the von Kármán and Bödewadt flows, to the specific value $\Omega_f=0.313\Omega_d$, so as to match the respective axial flows: the flux ejected from the stator balances the flux pumped towards the rotor. Let's note that in a cavity of finite radial extension, and thus in DNS's and experiments, the Batchelor solution collapses near the endwalls where strong fluxes (not shown on figure 2) ensure mass conservation between the two boundary layers (see for example in Refs. [39,40,51]).

(b) From Ekman boundary layer to rotating cavity flows

Even for large Reynolds numbers Re_h, the laminar, stationary, velocity field in a rotating cavity, where both disks rotate at the same angular velocity, retrieves a fluid in solid-body rotation. To observe boundary layers in a rotating cavity thus requires to alter the configuration, and the analytical approach to this laminar flow. Fifteen years before von Kármán, Ekman [49] had adopted a different approach to address the flow of a rotating fluid over a rotating disk. In the frame of reference rotating with the disk, at angular velocity Ω_d, assuming the dominance of the Coriolis term compared to the convective ones (which corresponds to $Ro=0$ in Eq.3.3) leads to a system of linear ordinary differential equations satisfied by the radial and azimuthal components of the velocity. The two-dimensional flow, perpendicular to the direction of rotation, solution to

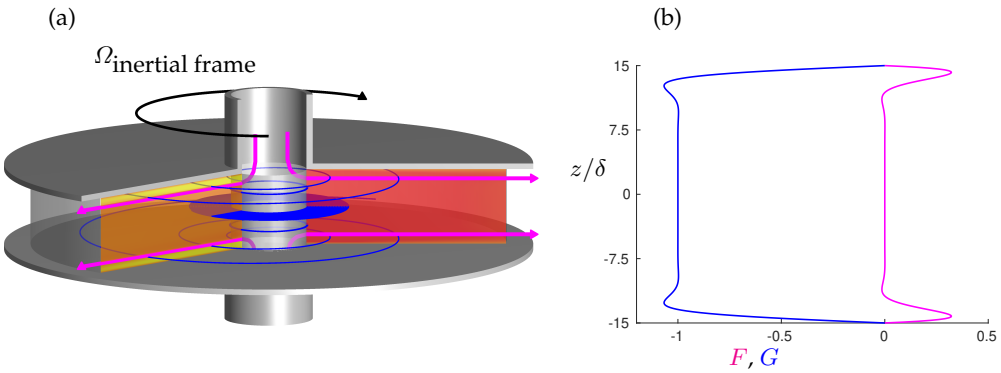

Figure 3: Rotating open cavity flow in the rotating frame of reference. (a) The meridional plan on the right shows the azimuthal component of the velocity and the one on the left the radial component. A few streamlines are depicted in blue and the imposed radial flux in magenta. (b) Axial shape functions F (magenta) and G (blue) of the velocity profile, as functions of z/δ.

this problem reads

$$\begin{aligned} u &= -V_g \exp\left(-\frac{z}{\delta}\right) \sin\left(\frac{z}{\delta}\right) \\ v &= V_g \left[1 - \exp\left(-\frac{z}{\delta}\right) \cos\left(\frac{z}{\delta}\right)\right], \end{aligned} \tag{2.6}$$

where $\delta = \sqrt{\nu/\Omega_d}$ and V_g is the geostrophic velocity at infinity, assumed here to be along the azimuthal direction. Unlike the von Kármán solution Eq.(2.1), the Ekman one Eq.(2.6) allows, and actually requires, an arbitrary geostrophic velocity V_g, potentially departing from a linear function of the radius r.

In a fashion similar to the rotor-stator flow, it is proposed to express the flow in a rotating cavity in the form of two mated Ekman boundary layers:

$$u = V_g(r) F\left(\frac{z}{\delta}\right) \text{ and } v = V_g(r) G\left(\frac{z}{\delta}\right), \tag{2.7}$$

with the axial shape functions

$$\begin{aligned} F &= -\left[\exp\left(-\frac{z+h/2}{\delta}\right) \sin\left(\frac{z+h/2}{\delta}\right) - \exp\left(\frac{z-h/2}{\delta}\right) \sin\left(\frac{z-h/2}{\delta}\right)\right] \\ G &= \left[1 - \exp\left(-\frac{z+h/2}{\delta}\right) \cos\left(\frac{z+h/2}{\delta}\right) - \exp\left(\frac{z-h/2}{\delta}\right) \cos\left(\frac{z-h/2}{\delta}\right)\right]. \end{aligned} \tag{2.8}$$

Rather than conceiving of the radial flow u imposed by the azimuthal one v driven by the geostrophic velocity V_g, an imposed radial flux Q is considered. The conservation of this flux along the radial direction then imposes the geostrophic velocity

$$V_g(r) = -\frac{Q}{\delta 2\pi r \left[1 - \exp(-h/\delta)\left(\cos(h/\delta) + \sin(h/\delta)\right)\right]} \approx -\frac{Q}{\delta 2\pi r} \text{ for } h \gg \delta, \tag{2.9}$$

which decreases as $1/r$. The continuity equation then imposes a null axial velocity $w = 0$ everywhere in the cavity. By directly feeding the radial centrifugal flow along the disks, this radial flux Q fosters the boundary layers and prevents the solid-body rotation of the fluid. Observing this flow in a finite-radius cavity, and, therefore in a DNS, requires to impose the radial flow at the specific radii of the shaft and shroud, as shown by the magenta arrows in figure 3. Ideally, this imposed profile, beyond the Ekman profile, should also take into account non-linearities, as in [43,52]. Imposing a less specific profile at the shaft induces a "healing length" along the radial direction to match this profile to the Ekman solution, as argued in [8] and numerically observed in [47].

3. Characteristic flow parameters

Addressing the previous theoretical base flows and their stability analyses in regard to experimental set-ups and DNS's require to introduce several local and global dimensionless parameters.

In the single disk configuration, to cover cases of rotating disks in stationary fluids, of stationary disks in rotating fluids and everything in-between, Faller [20] proposed to define a common reference rotation rate as

$$\widetilde{\Omega} \equiv \frac{1}{4}(\Omega_f + \Omega_d) + \sqrt{(\frac{1}{4}(\Omega_f + \Omega_d))^2 + (\frac{\sqrt{2}}{2}(\Omega_f - \Omega_d))^2}. \tag{3.1}$$

The flow over an infinite single disk then solely depends on a and self-similarity variable

$$Re_r = \frac{r}{\delta} = r\sqrt{\frac{\widetilde{\Omega}}{\nu}}, \tag{3.2}$$

with the boundary layer thickness $\delta = \sqrt{\nu/\widetilde{\Omega}}$, and the dimensionless parameter

$$Ro = \frac{\Omega_f - \Omega_d}{\widetilde{\Omega}}, \tag{3.3}$$

scaling the ratio between the rotation rate of the fluid far from the disk and the rotation rate of the system. In the case of an infinite disk rotating in a still fluid, $Ro = -1$ and is construed as a Rossby number: in the frame rotating with the disk, it compares the (nonlinear) inertial effects to the (linear) Coriolis force ($Ro \equiv \|\boldsymbol{V} \cdot \boldsymbol{\nabla} \boldsymbol{V}\| / 2 \|\boldsymbol{\Omega}_d \wedge \boldsymbol{V})\|$). In the case of a stationary infinite disk in a rotating fluid, $Ro = +1$, but can hardly be interpreted as a Rossby number. It is nonetheless customary to call Ro the Rossby number of the flow, and this number is constant for for flows over infinite single disks. Besides Ro, the instability of this flow is also quantified by a local Reynolds number, based on the boundary layer thickness and an external velocity in the rotating frame, the so-called geostrophic velocity V_g:

$$Re_\delta = \frac{\delta\, V_g}{\nu}. \tag{3.4}$$

Over infinite single disks, one can assume $V_g = \left(\Omega_f - \Omega_d\right) = \Delta\Omega r$ so that the Reynolds number reads:

$$Re_\delta = \frac{\delta\, \Delta\Omega\, r}{\nu} = Ro\, Re_r, \tag{3.5}$$

and increases linearly with the radius r.

For rotating disks of finite radius R_{out}, the global Reynolds number

$$Re = \frac{\Omega_d\, R_{out}^2}{\nu} \tag{3.6}$$

can be formed for comparison purposes and also because, as a superior bound for Re_r, it controls the possibility to observe instabilities developing on the rotating disk.

In cavities [45,52], the geometry is fully characterized by two parameters, the aspect ratio $\Gamma = h/\Delta R$, and the curvature parameter $R_m = (R_{out} + R_{in})/\Delta R$, with $\Delta R = R_{out} - R_{in}$. In cylindrical cavities with no inner shaft, $\Gamma = h/R_{out}$ and $R_m = 1$. Besides the global Reynolds number above, the flow is also characterized by

$$Re_h = \left(\frac{h}{\delta}\right)^2, \tag{3.7}$$

which controls the separation between the upper and lower boundary layers. In cavities without inner shaft, this vertical Reynolds number relates to the global one by $Re_h = Re\,\Gamma^2$. For large Re_h, the Rossby number remains a relevant parameter. It is nonetheless computed assuming the flow is quasi-geostrophic in the central region far from the boundary layers and relating the geostrophic velocity $V_g = \Delta\Omega\, r$ to a local rotation rate Ω_f of the fluid measured at midheight.

Configurations	Global parameters	Local parameters
Single disk	$Re = \frac{\Omega_d R_{out}^2}{\nu}$ $Ro = \frac{\Delta\Omega}{\widetilde{\Omega}}$	$Re_r = \frac{r}{\delta} = r\sqrt{\frac{\widetilde{\Omega}}{\nu}}$, $Re_\delta = \frac{\delta\,\lvert\Delta\Omega\rvert\, r}{\nu} = \lvert Ro\rvert\ Re_r$
Open rotating cavity with radial through-flow	$Re = \frac{\Omega_d R_{out}^2}{\nu}$, $Re_h = \left(\frac{h}{\delta_d}\right)^2$	$Re_\delta = \frac{\lvert Q\rvert}{2\pi r\nu}$, $Ro = -\frac{Q}{\delta\, 2\pi r^2\, \Omega_d}$
Rotor-stator cavity	$Re = \frac{\Omega_d R_{out}^2}{\nu}$, $Re_h = \left(\frac{h}{\delta_d}\right)^2$	$Re_r = \frac{r}{\delta}$, $Ro = \frac{V_g(r)}{\widetilde{\Omega}\, r}$

Table 1: Definitions of global and local control parameters used in the literature to characterize the flow of a fluid of viscosity ν depending on the geometrical configuration. h, R_{in}, R_{out} are the height, the inner and outer radius, respectively. Ω_d is the rotation rate of the disk and Q is the dimensional volume flow rate. $\delta_d \equiv (\nu/\Omega_d)^{1/2}$ and $\delta \equiv (\nu/\widetilde{\Omega})^{1/2}$ correspond to the definitions of the characteristic viscous lengths.

Due to edge effects, laminar flows over disks and in cavities of finite radius tend to depart from the self-similar solution, the local rotation rate of the fluid Ω_f is usually found to vary along the radial direction and so does the Rossby number. Besides, in open cavities with radial through-flow, the geostrophic velocity V_g is imposed by the through-flow, as given by equation (2.9) and the Rossby number varies accordingly as $1/r^2$.

In , the stability of the flow is thus governed by a global Rossby number $Ro = \mathrm{cste}$ and by the local Reynolds numbers Re_δ or Re_r. In finite-radius systems, due to the radial inhomogeneity of the flow, the stability properties are governed by local Rossby and Reynolds numbers, both varying with the radius. that require a global stability analysis. These global and local parameters are summarized in Table 1.

4. Rotating disk boundary layer instabilities

The stability of flows in cavities of small aspect ratio ($\Gamma \ll 1$) and large Re_h is governed by the stability of the boundary layers above the disks, and thus akin to the instability mechanisms found in single disk configurations. Flows above the cavity walls fit in the broad category of shear flows, in the sense that at least one velocity component varies in the wall-normal direction. As such, they are subject to different types of instabilities that are generic for rotating disk flows, and which are usually named in the literature according to their chronological order of discovery, the so-called type-I, type-II and type-III instabilities. They take the form of vortex rolls within the boundary layers, expanding in spirals arms or circular waves centered on the rotation axis (both can even coexist in the same boundary layer), as illustrated on the examples of Figure 4 in a rotor-stator cavity. In such a closed rotor-stator cavity, however, other instability mechanisms can be involved within the vertical boundary layer along the shroud, and along the shaft in annular configurations. These will not be discussed in this review as they play a rather secondary role in the transition to turbulence in small aspect ratio cavities, mostly acting as perturbations and slightly shifting the threshold of occurrence of the main instabilities of the rotating disk boundary

layers (see [46] for more details on the stability of the vertical boundary layer in tall cavities, at $\Gamma \gg 1$).

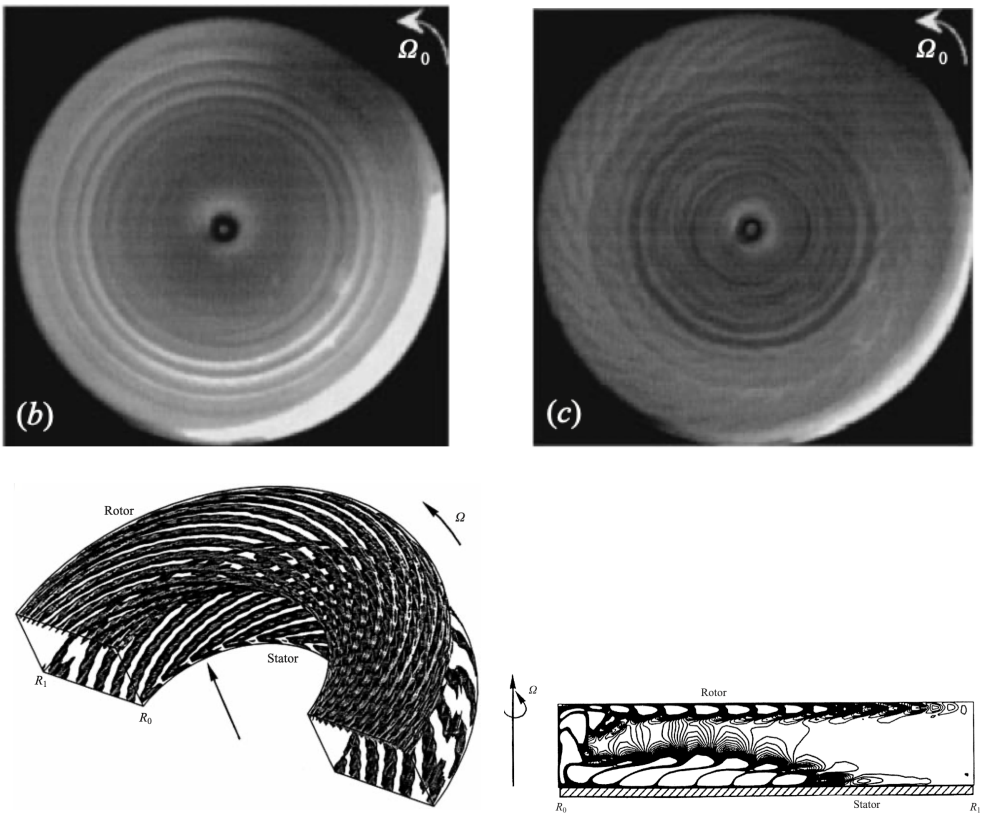

Figure 4: Examples of patterns for the generic type-I and type-II instabilities in a rotor-stator cavity. (Top) Experimental visualizations of circular waves alone at $Re_h = 120$ (left), and circular waves and spiral arms at $Re_h = 180$ (right) in the inward boundary layer close to the stationary disk, an extract of Figure 4 of Ref. [53]. (Bottom) Three-dimensional numerical solution at $Re_h = 330$ in an annular cavity ($R_m = 5$, $\Gamma = 0.2$), exhibiting spiral arms in both boundary layers (left), and the corresponding vortical structures circulating clockwise in the meridional plane $(r, z, \pi/4)$ (right), a copy of Figure 9 of Ref. [45].

The first description in the literature of an instability developing in a rotating disk boundary layer was by Gregory *et al.* [15], who observed the — now called — type-I instability in a von Kármán boundary layer. Faller [17] later observed the same type-I instability in an Ekman-type boundary layer. Type-II rolls are more elusive and were first reported in [18,19]. Whereas the type-I instability originates in the inflectional nature of the azimuthal velocity profile (hence it is often labelled "crossflow instability"), the type-II instability results from the combined effects of viscosity, Coriolis force (when computed in the frame rotating with the disk) and streamwise curvature. Lilly [16] proposed the first linear stability analysis, including viscous and Coriolis terms, in the Ekman boundary layer, evidencing two families of instabilities with distinct critical Reynolds numbers and corresponding to type-I and type-II instabilities. The type-III have only been predicted by spatial stability analyses [54] and have never been reported experimentally. They were found to propagate inwards, towards the disk center, and, albeit strongly damped, they are a theoretical necessity to obtain absolute type-I instabilities, addressed in the forthcoming.

To conform with the observed patterns and are characterized and identified by three modal parameters: the azimuthal wavenumber β, the radial wavelength λ_r and the temporal frequency ω. These instabilities develop beyond a critical Reynolds number $Re_\delta^c = Re_r^c\ |Ro|$, which therefore amounts to a critical radius Re_r^c. Combining Re_r^c β and λ_r, they are also characterized by ϵ° the orientation of the spiralling arms with respect to the tangential direction. It has been observed that Re_r^c depends linearly on the Rossby number, which ranges from -1 to 1, depending on the boundary layer as discussed in Sec 2. Tatro and Mollo-Christensen [18] proposed the following laws for type-I and type-II critical Reynolds number Re_r^c :

$$\begin{aligned} Re_r^{c,\mathrm{I}} &= 124.5 - 7.32\,Ro \\ Re_r^{c,\mathrm{II}} &= 56.3 - 116.8\,Ro \end{aligned} \tag{4.1}$$

Also, the most unstable azimuthal wavenumber β_{max} was theoretically found to vary linearly with Re_r/Ro by Lingwood [23]. A compilation of characteristic parameter values extracted from the literature for type-I and II instabilities is provided in Tables 2, 3 and 4, for the single disk configuration. These values are obtained experimentally (XP), or theoretically by linear stability analysis (LSA) of the family of similitude solutions, computed for different Rossby numbers.

Authors	Method	Ro	λ_r/δ	β	ω/Ω	ϵ°	Re_r^c
[16,20,23,37,38]	LSA	0	11.49–11.9	-	0–5.84	6.9-14.5	110–116
[23]	LSA	-0.5	13.5	38	0	14.1	160.9
[20,23,37,55]	LSA	-1	15.3–17	23–27	0–2.19	10.9–14.35	281–290.1
[17,18]	XP	0	9.6–12.7	-	-	10–16	124.5–125
[29,56]	XP	-1	17.7	22–39	1.17	11–14	285–300

Table 2: Sample values from the literature for critical modal parameters and Reynolds number of convective type-I instabilities in the boundary layers of a single disk. (XP) and (LSA) stand for experiments and linear stability analysis, respectively.

Authors	Method	Ro	λ_r/δ	β	ω/Ω	ϵ°	Re_r^c
[38]	LSA	1	16.11	-	-	-27.38	18.9
[16,20,37]	LSA	0	21–24	-	10.56	-23.3–-20	54.2–55
[20,23,37]	LSA	-1	18–26.91	6–7	7.88–8.17	-19–-24.7	64.4–85.3
[18]	XP	0	25–33	-	-	-8–0	56.3

Table 3: Same as Table 2, for convective type-II instabilities.

Authors	Method	Ro	λ_r/δ	β	ω/Ω	ϵ°	Re_r^c
[23,55,57]	LSA	-1	28.95	68	17.7	31.4–31.9	[507.3; 507.4]
[23]	LSA	-0.8	24.93	84	21.6	31.6	434.8
[23]	LSA	-0.6	21.37	100	24	29.9	345.4
[23]	LSA	0	16.57	92	20.13	-	198
[23,38]	LSA	1	23	-59–-56	107–110.6	-	21.6–21.7

Table 4: Same as Table 2, for absolute type-I instabilities.

Authors	Type	Method	Ro	λ_r/δ	β	ω/Ω	ϵ°	Re_r^c
[38]	I	LSA	0	11.5	-	5.84	7.2	112.8
[38]	I	LSA	-0.75	15.06	-	2.19	10.9	278.6
[52]	I	DNS	-	11–15	-	1.9	7	-
[38]	II	LSA	0	21.66	-	10.56	-23.4	54.18
[38]	II	LSA	-0.75	28.56	-	8.73	-26.3	90.23
[47]	II	DNS	-	26–29	0	4.86	0	74–112
[52]	II	DNS	-	17–32	-	9	-20	-
[38]	I absolute	LSA	0.687	33	16	14	-	48.5
[52]	I absolute	DNS	-0.83	29–31	68	17.23	30	442

Table 5: Sample values from the literature for modal parameters and critical Reynolds number of type-I, type-II and type-I absolute modes in the boundary layers of the rotating disk in a cavity. LSA and DNS stand for linear stability analysis and direct numerical simulation, respectively. LSA results are obtained either using the Batchelor base flow for infinite radius rotor-stator cavities or using the local mean flow velocity profiles calculated from DNS of the full Navier-Stokes equations in finite radius cavities.

Unlike flows over single disks, rotating cavities exhibit a radially varying rotation rate of the fluid at mid-height, leading to consider a radially varying Rossby number (see in Sec. 2 and also definitions in Table 1). In closed rotor-stator cavities, this is particularly true in the flow regions near the edge of the boundary layers, in the vicinity of the shroud and shaft, if present [44,45,51]. In open rotating cavities with throughflow, this is true over the entire radius in order to conserve the radial mass flow rate [52]. It must be noted in this latter configuration that, while the local Reynolds number Re_δ decreases with r as $1/r$ in the radial outward direction (unlike the single-disk configuration where it increases as r), the local Rossby number decreases as $1/r^2$, and so does the critical Reynolds number Re_δ^c, and the flow remains unstable beyond a critical radius Re_r^c. This form of spatial (radial) inhomogeneity is specific to cavity flows, compared to single-disk flows. This restricts the validity of scalings (4.1), and, more generally, of all linear stability analysis, to a local viewpoint, and differentiates the stability of the cavities from that of single disks. A compilation of characteristic parameter values in cavities is provided in Table 5.

Discrepancies soon arose between experiments and linear stability analyses regarding the number of spiralling arms, i.e. the azimuthal wavenumber β, the dominance of stationary modes and the fact that type-II instabilities were rarely observed despite having the lowest critical Reynolds number. It is generally agreed (see the review [58]) that stationary modes actually result from a forcing by surface roughness, while travelling modes are due to impulsive or incoming-flow perturbations. The fact that, despite having a lower critical Reynolds number, the type-II instability modes have a lower growth rate is often invoked to explain why they are dominated in the experiments. An alternative explanation put forth the receptivity of the boundary layer [23,59]. The difference between the azimuthal wavenumbers observed experimentally and the most unstable one predicted theoretically, would result from the superposition of several wavenumbers, associated with a random roughness distribution on the disk.

A more recent theoretical approach to the stability of these boundary layers has shed new light on the transition process to turbulence, to be further discussed in the next section. It considers the impulse response to a brief and radially localized perturbation in the boundary layer. This amounts to the convective/absolute stability analysis, introduced in fluid mechanics by Huerre & Monkewitz [60] for open homogeneous flows, such as Taylor–Couette or Rayleigh–Bénard cells with superimposed Poiseuille flows. This analysis classifies the behaviour of these flows as unconditionally stable, convectively unstable and absolutely unstable. An unconditionally stable

flow is characterized by any perturbation to the flow decaying. In a convectively unstable flow, a localized perturbation will grow in space and time but is also advected downstream such that it eventually wash out of finite-length domains. Without an extrinsic permanent source of perturbations, the system returns to the base flow everywhere. In contrast, an absolutely unstable flow is characterized by localized perturbations that grow and spread both upstream and downstream, spontaneously invade the whole domain and imposes its own, intrinsic, behaviour. An absolute instability arises when an unstable mode is found to present both to a positive temporal growth rate and a null group velocity. Flows over rotating disks and in rotating cavities, however, are not homogeneous flows as they evolve along the radial direction. Convective/absolute stability analysis nonetheless provides a usefull framework to address the local behaviour of perturbations, parameterized by the local Rossby and Reynolds numbers, and the spatio-temporal diagrams on Figure 5 exemplify the convective (panel a) and absolute (panel b) responses of the rotating disk boundary layer, in the case of an open cavity sector with radial throughflow [52]. Moreover, the local convective/absolute stability analysis paves the way to

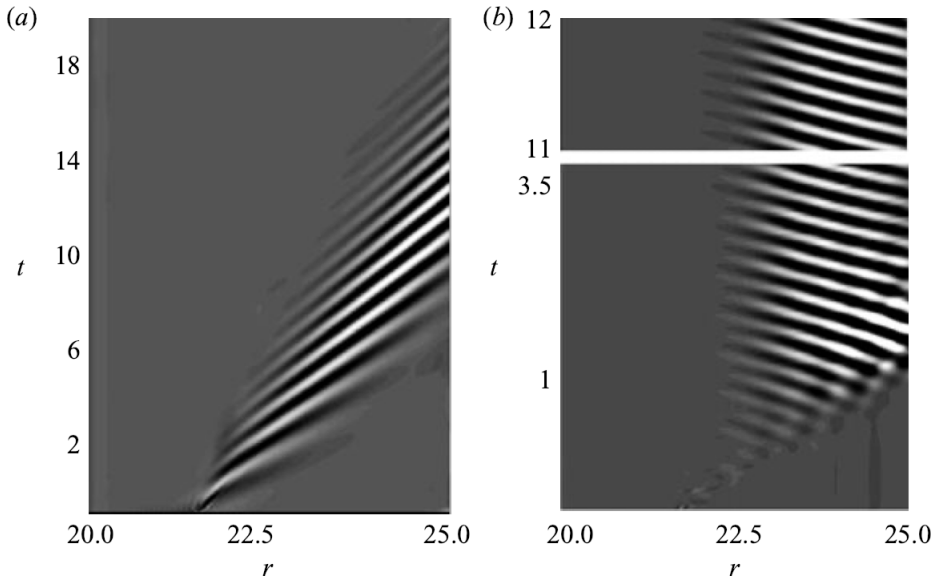

Figure 5: Spatio-temporal diagrams illustrating the impulse response of the boundary layer in the rotating disk cavity with radial throughflow: (a): Flow convectively unstable everywhere, for $94 \leq Re_\delta \leq 118$ and $-0.22 \leq Ro \leq -0.14$. (b): Flow with an absolutely unstable region, leading to a global mode, for $390 \leq Re_\delta \leq 490$ and $-0.91 \leq Ro \leq -0.64$. Direct numerical simulations of full Navier-Stokes equations, a copy of Figure 4 of Ref. [52].

figure out how the varying dynamics of a perturbation over the whole disk "hang together" to build up a global mode of instability. Indeed, analytical approach to global modes builds on how absolute instabilities travel and saturate over a radially varying base flow and look for a specific radial location that can act as a wavemaker and govern the global mode by imposing its critical conditions and frequency.

Lingwood [21–23] was the first to investigate the convective/absolute nature of the instabilities in the single disk boundary layer, both theoretically and experimentally. Whereas further studies have confirmed these local linear stability results and the existence of an absolute instability (see [27,38,61] for instance), no general agreement exists concerning their outcome in terms of global behaviour of the instabilities, as the development of the flow along the radial direction is taken into account. Existing works show a competition between stabilizing non-parallel effects and destabilizing non-linear ones. Indeed, whereas transient absolute behaviour was observed

by Davies and Carpenter [27] from simulations of linearized Navier-Stokes equations, it was not sustained in time. Convective behaviour eventually dominated, and locally the perturbations relaxed to zero. This behaviour was experimentally confirmed by Othman and Corke [29], using a sufficiently low-amplitude initial pulse-jet excitation to remain in the linear regime of the instabilities, therefore demonstrating the linear global stability of the rotating disk boundary layer. Davies *et al.* [28] later showed that non-parallel effects led to a strong detuning, i.e. the flow being absolutely unstable, the radial variations of the local absolute frequency might be sufficiently stabilizing the global frequency to maintain a linear global stability. Couairon and Chomaz [62], however, showed in a more general framework that when non-linearities are taken into account the presence of an absolutely unstable region is a sufficient condition for the existence of a fully non-linear global mode in the lee of a steep front localized at the upstream limit of the absolutely unstable zone, a so-called elephant mode. In the rotating disk boundary layer, Pier [55] showed the possible existence of such a global non-linear elephant mode at the onset of local absolute instability. In this situation, the destabilizing effect of the non-linearities is stronger than the stabilizing effect (or detuning) of spatial inhomogeneity. The flow is locally absolutely unstable and globally non-linearly unstable while it may remain globally linearly stable. This flow feature would imply the existence of a subcritical global bifurcation, which was demonstrated in the angular sector of an open cavity between two co-rotating disks by Viaud *et al.* [52] using DNS, and later in the infinite single disk case by Appelquist *et al.* [31] using linearized DNS. These works further evolved into studies where roughness [26,29,63] or the edge of the disk in finite-size system [31–33,64] would act as wavemaker, instead of the front beating at the local absolute frequency and wavelength.

The convective/absolute analysis of the disk boundary layers has been extended to the rotor-stator cavity [38,44] and to the rotating cavities with throughflow [52], by performing both linear stability analyses and direct numerical simulations of the full Navier-Stokes equations. As mentioned above for the spatial analysis of type-I and type-II instabilities, the convective/absolute analysis provides results rather similar to the single disk configuration (Tables 2, 3, 4, 5).

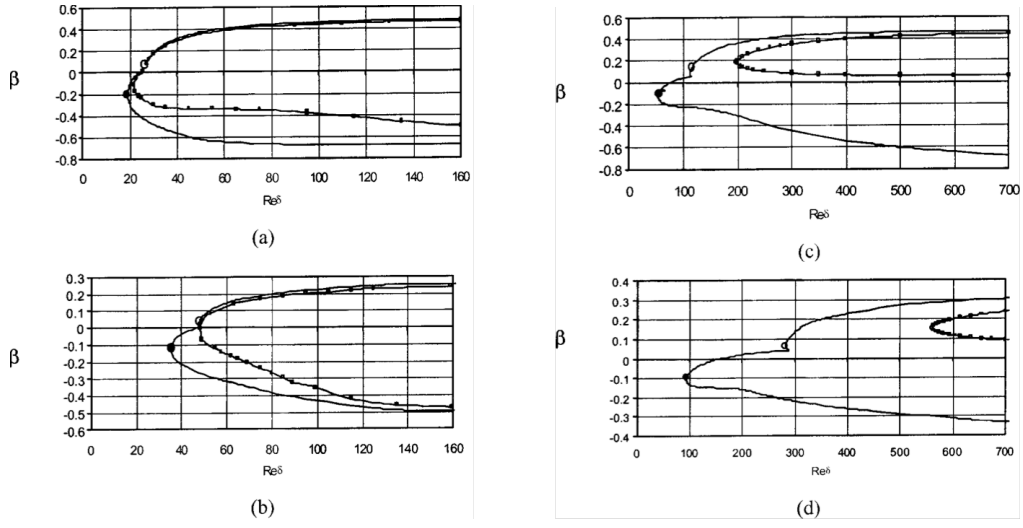

Figure 6: Linear stability results. Comparison of the neutral curves $\beta = f(Re_r)$ of the absolutely (black squares) and convectively (solid line) unstable flow obtained for the Bödewadt similarity solution above a single disk (a), the stationary disk boundary layer in a rotor-stator Batchelor flow (b), the Ekman similarity solution above a single disk (c) and the rotating disk boundary layer in a rotor-stator Batchelor flow (d). The critical points of type I and type II are marked by the white and black dots, respectively. A copy of Figure 7 of Ref. [38].

Serre *et al.* [38] performed the convective/absolute analysis of the Batchelor solution in a rotor-stator cavity of infinite radius. Results are provided in Figure 6 in the form of critical Reynolds numbers Re_r^c as functions of azimuthal wavenumber β, and compared to single disk configurations. As for these latter, the stationary disk boundary layer is substantially more unstable than the rotating disk one, and rapidly becomes absolutely unstable at very small Reynolds numbers (Figures 6a, b), the absolutely unstable domain almost overlapping the convectively unstable one. The rotating disk boundary layer in the rotor-stator cavity (Figure 6c, d) was found to be more stable than the Ekman boundary layer, as expected from (4.1), and the transition to absolute instability is strongly postponed with a critical Reynolds number almost three times larger. These differences could actually be accounted for by the different Rossby numbers, with $Ro = 0$ in the Ekman solution and $Ro = -0.687$ in the Batchelor solution. These results suggest that the stationary disk boundary layer is likely to be the first to transition to turbulence, while the rotating disk boundary layer will require higher rotation rates to breakdown to turbulence (see next section Sec. 5 for further discussions).

Considering now a finite size rotor-stator configuration, Yim *et al.* [44] performed a convective/absolute stability analysis of the local mean velocity profiles obtained by direct numerical simulations of the full Navier-Stokes equations. The results confirmed those obtained in infinite radius configuration, but showed for the stability of the rotating disk boundary layer an impact of the edge of the disk on the convective/absolute stability analysis. Indeed, the mean velocity profiles in the cavity increasingly depart from the von Kármán solution as this edge is approached, which leads to a boundary layer more unstable than predicted by the LSA of the self-similarity solution calculated at the same Rossby number. More specifically, the critical Reynolds number for the convective/absolute transition $Re_\delta^{c/a}$ was found to be smaller than for the equivalent von Kármán solution at the same Rossby number. In the DNS, this was observed to induce a very unstable flow at the edge, associated with strong fluctuations observed at all investigated global Reynolds numbers. Moreover, for annular rotor-stator configurations with an inner radius located in the absolutely unstable region of the stationary disk boundary layer, the latter can act as a wavemaker continuously disturbing the rotating disk boundary layer and, thus, leading to convectively unstable rolls travelling outwards in the direction of the mean radial flow. This is clearly shown in all DNS results of the literature (see for example in Ref. [45]).

5. The current debate on the transition scenarios

Beyond its theoretical interest, understanding and characterising the mechanisms of transition to turbulence, and ultimately controlling them, is of practical interest in many industrial devices, where increasing or decreasing heat and mass transfers or mixing by turbulence can improve performance.

Lingwood's theoretical local linear stability analyses [21] were pioneering in suggesting a direct route to turbulence driven by absolute instabilities. The notable collapse of the experimental transition Reynolds numbers found in the literature for the von Kármán flow around the value $Re_\delta = 513$ seems to confirm this direct route. Indeed, even though some later work [29] advocated the appearance of a delayed transition, the survey done by Imayama *et al.* [33] concluded that, provided a common criterion for transition is used, all clean-disk experiments show a transition between $Re_\delta = 508$ and $Re_\delta = 515$, while the flow becomes fully turbulent around $Re_\delta = 650$.

Although the direct route scenario has been supported by a large body of experimental results, Lingwood's initial scenario based on local dynamics does not take into account two characteristics of these flows in finite-size systems, namely spatial inhomogeneity and non-linearity, which require global non-linear stability analyses. In this context, the results show that linear and non-linear mechanisms compete, and that the rotating-disk boundary layer is both locally absolutely unstable [21], globally linearly stable [27] and globally non-linearly unstable [65]. The discrepancy observed between the global linear and non-linear dynamics is mainly induced by the large convectively unstable region upstream of the absolutely unstable region.

Thus, even small external perturbations on the disk or in the surrounding, as in the finite-size cavities, may undergo a strong transient amplification and trigger non-linear dynamics. All these features and mechanisms in competition have led to much of the work on the study of the transition to turbulence, resulting in a large body of work focusing mostly on single rotating disk configurations (complete references and results are provided in recent papers by [13,63,66]), while much less efforts have been dedicated to cavities, see in Refs. [43,44,52]. The results and scenarios found in the single disk configurations can, however, be completed, and used as a backbone for scenarios in cavities.

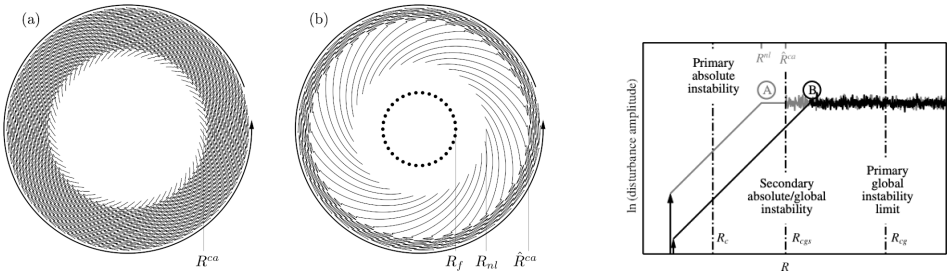

Figure 7: Sketches showing the two classes of transition scenario in the single-disk configuration: (a) The *absolute* scenario: onset of a primary absolute instability characterized by a steep front and spiral arms immediately followed downstream by secondary absolute instability and turbulence. (b) The *convective* scenario: onset of a primary convective instability excited by self-sustained perturbations, nonlinear saturation and secondary absolute instability downstream leading to turbulence. (c) In the *convective* scenario, transition to turbulence for disturbances with two different amplitudes. (a, b) a copy of Figure 3 of Ref. [67]. (c) A copy of Figure of Ref. [63]. R^{ca}, R_f, R^{nl}, and $\hat{R}^{ca}$ denote respectively the critical Reynolds numbers of the local absolute primary instability, of the forcing, of the nonlinear saturation of the primary convective instability and of the absolute global secondary instability.

To date, although no detailed description of the complete process of transition exists in the literature, two main routes to turbulence seem to emerge in single-disk configurations involving a primary and secondary instability, called *convective* or *absolute* depending on the nature of the dominant mechanism, Fig.7. Even though they are both based on the existence of an absolutely unstable zone of sufficient radial extent, the former requires external forcing while the latter is self-sustained.

(i) The *convective* scenario as in Ref. [20,22,26,63,67–70]. As mentioned in Sec. 4, the rotating disk boundary layer is convectively unstable over the radial interval $284 < Re_\delta < Re_\delta^{c/a} \simeq 507$ and can thus act as an amplifier of some sustained external perturbations. For turbulence to occur, it is assumed here that the non-linear saturated state occurs prior to R_{out}. In such a scenario, a primary convective instability saturates non-linearly, and becomes itself absolutely unstable with respect to a secondary instability, eventually leading to turbulence (Fig. 7b). In experiments [20,26,68,69], theory [22,67] and numerics [63], this scenario is selected and investigated by implementing a radially localized forcing whose the frequency, azimuthal wavenumber and amplitude can be changed. The forcing amplitude in DNS or the roughness height in experiments determines the radius of the transition, as illustrated on Fig. 7(c). An increase/decrease of the forcing amplitude then brings about earlier/later transition. Indeed, depending on the radius at which the primary rolls has grown large enough to become susceptible to a secondary global instability, transition occurs immediately at the theoretical position of the secondary front (A) or slightly downstream (B).

(ii) The *absolute* scenario as in Ref. [31–33,61,64,67,71]. It is observed in the absence of any external perturbation, and for travelling cross-flow waves (type-I instability) when the region of absolute instability is large enough before the outer edge R_{out}. Depending on flow conditions, this scenario is found to be as sub- or supercritical.
The supercritical scenario is driven by the linear global instability as a first step in the onset of transition, as in Ref. [31–33,61,64]. This occurs in disk of finite radial extension when R_{out} is large enough for the global flow to be linearly unstable, typically $R_{out} > Re_\delta = 594$ (compared with the critical Reynolds number for absolute instability of 507). In this condition, there is a mechanism for a supercritical global bifurcation whereby infinitesimal initial perturbations can trigger a linear global mode. with a steep front driven by the local absolute instability. This latter is generated either at finite radial edge of the disk, as argued in Ref. [64] using the linearized complex Ginzburg–Landau equation with weakly spatial variation, or at the end of the linear domain as obtained numerically from linearized Navier-Stokes equations by Appelquist *et al.* [61] by modeling a turbulent outer ring. In such scenario , the rotating-disk flow is linearly globally unstable and the linear global mode leads directly to a nonlinear global mode.
The subcritical scenario is driven by a non-linear global instability as a first step in the onset of transition, as proposed in Ref. [55,67]. The flow responds to any strong enough impulse perturbation through a steep global "elephant mode" (non-linearly globally unstable), positioned at the upstream limit of the absolutely unstable zone ($Re_\delta^{c/a} = 507$). This primary global elephant mode is itself already absolutely unstable to secondary instabilities [55,72] and direct transition follows, Fig. 7(a). Note that it can be observed in finite-disk system for R_{out} below 594. In the frame of linear global stability, this scenario is called subcritical since only large-amplitude perturbations can trigger the global mode due to the competition between the stabilizing nonparallel effects and the absolute instability.
Recent work by Lee *et al.* [66], however, suggests something different. This numerical investigation of the impulse response of a clean disk of finite extent, including some on-demand relaminarization of the turbulent zone concludes to the presence of 32 stationary vortices without permanent forcing, that they are dominated by their travelling harmonic, and to the presence of a wavemaker somewhere between 611 and 630, independent of the turbulent zone and the radial confinement it induces.

All these findings show the complexity of the scenarios, and stress the importance of the nature (permanent or impulse) as well as the intensity of the forcing, and of the confinement, beyond the role of the single control parameter Re. This complexity is further increased in cavities, where flow regions with different characteristics and stability properties coexist. However, the study of the above-mentioned transition scenarios in this deceptively simple single-disk configuration sheds light on their study in cavity configurations, and more specifically in the closed rotor-stator cavity as well as in the open rotating cavity with radial throughflow introduced in Sec. 2.

In the rotor-stator cavity (Fig. 8), turbulence first occurs in the stator boundary layer, as it could be expected from the stability analysis in Sec. 4. This has been shown both numerically [73–76] and experimentally [76–78]. To our knowledge, no transition scenario has ever been identified in the stator boundary layer, due to the swift development of turbulence. Experiments carried out by Cros *et al.* [78] are certainly the only ones to provide some insight on the transition mechanisms for moderate Reynolds numbers, up to $Re = 73890$, through non-linear interactions of type-I and type-II modes identified at lower rotation rates. Type-I and type-II instabilities are characterized by annular and spiral arms patterns which can propagate inward into the boundary layer with decreasing intensity (Fig. 8). These authors reported, at $Re = 32840$, only one period-doubling bifurcation before its complete destruction by transition to wave turbulence. No relation between the bifurcation and the appearance of phase defects could however be determined.

Compared to the stator boundary layer, the transition in the rotating disk boundary layer occurs at much higher Reynolds numbers in both configurations of cavities addressed here. To our knowledge only numerical works exist in the literature (see complete references in recent works of [44,76]) and the results provided are still incomplete due to the very high mesh resolution required.

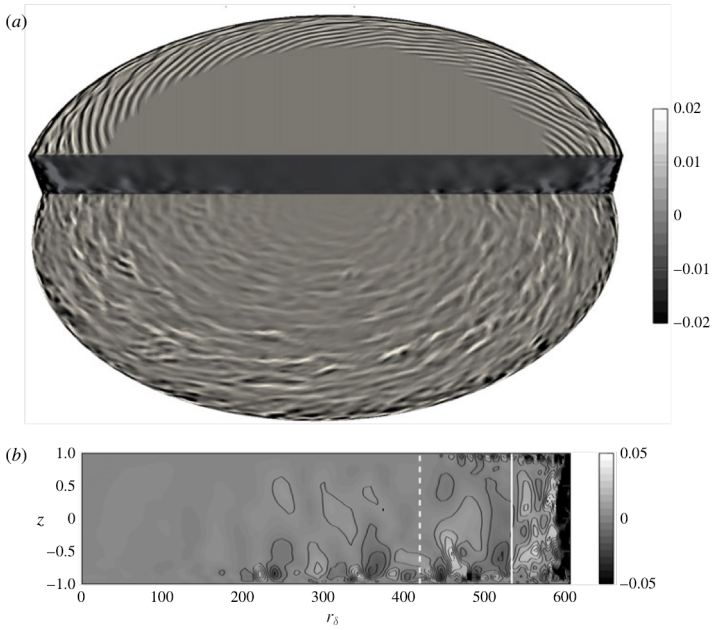

Figure 8: Transition to turbulence in a cylindrical rotor-stator cavity, a copy of Figure 3 of Ref. [44]. Instantaneous flow pattern in the whole cavity for $Re = 4 \times 10^5$. The stator is below. Iso-surfaces and iso-contours of the instantaneous axial velocity w. (a) Three-dimensional view. (b) Meridian plane. The white dashed and solid lines in (b) show the position of the spiral pattern (primary front) at $Re_\delta \approx 420$ and the beginning of the turbulent region for $Re_\delta \approx 538$.

If self-sustained perturbations are produced in the flow, transition to turbulence can occur at a lower Reynolds number than found for the clean single disk. In this case, a front composed by spiral arms may appear upstream of the local convective/absolute boundary predicted by local stability analysis. In the literature, these perturbations can emanate either from the very unstable stator layer in annular cavity [73,76] or be produced at the the rotor edge [44] where the flow is modified by the presence of a stationary shroud at R_{out}. Indeed, recent LES results of Makino *et al.* [76] suggest that the rotor boundary layer is perturbed due to disturbances emanating from the stator side, along the shaft. The convective mode of instability, identified in this work to type-II, is then excited and followed downstream by a secondary instability leading to the transition to turbulence at $Re_\delta \approx 470$ (see Fig. 9). It is however interesting to note that if the existence of a shaft promotes the transition to turbulence, it does not seem to affect the global scenario mechanisms, as similar results are obtained in a cylindrical rotor-stator cavity, but at higher Reynolds numbers (see again Fig. 9). This means that in this work, although the shaft promotes the advection of disturbances emanating from the stator, self-sustained disturbances still exist in the latter to excite a convective type-II instability in the rotor boundary layer. According to the classification proposed in the literature for the single-disk rotating boundary layer, this scenario falls into the category of the *convective* scenarios, as reported by Faller [20] and more recently by Imayama *et al.* [26] for a disturbed boundary layer. Note, however, that in the case of Faller and Makino *et*

al., the scenario is dominated by a type-II instability whereas a type-I is observed in the work of Imayama *et al.*.

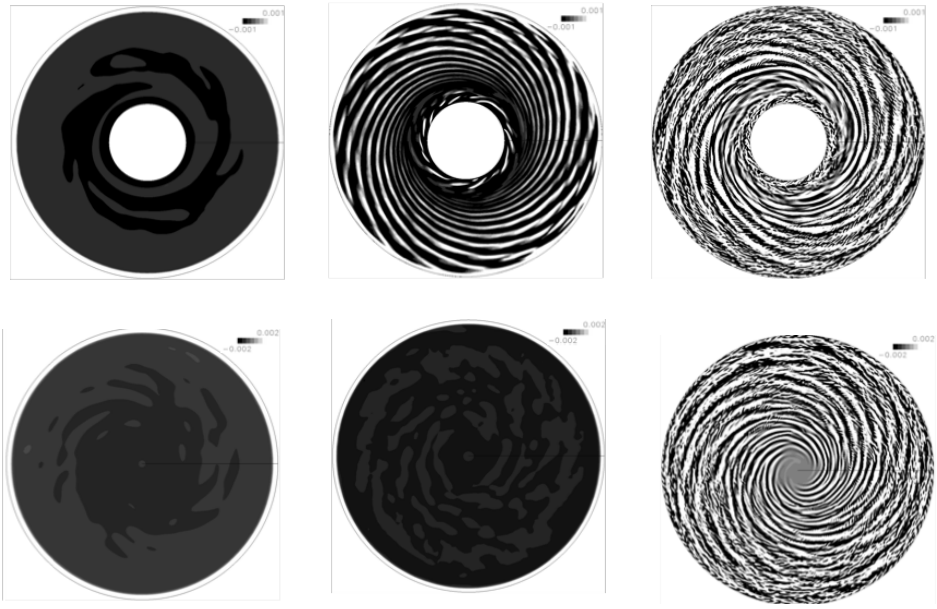

Figure 9: Instantaneous snapshots of the vertical velocity obtained by LES in the rotating disk boundary layer of an annular (top) ($R_m = 1.8$) and cylindrical (bottom) ($R_m = 1$) rotor-stator cavity of aspect ratio $\Gamma = 5$. Transition to turbulence: $Re = 4 \times 10^4$; $Re = 10^5$; $Re = 4 \times 10^5$ from the left to the right. A copy of Figure 10 of Ref. [76].

In the cylindrical rotor-stator cavity of Yim *et al.* [44], the transition seems however to differ and to be dominated at moderate rotation rates by strong fluctuations observed at the rotor edge ($Re_\delta \approx 420$) (see Fig.10), within a region where the flow modified by the presence of a stationary shroud, is no longer similar to the von Kármán boundary layer, and where shear and centrifugal effects cause a strong instability as mentioned in the single disk configuration by Pier [32]. These fluctuations act as a strong source of noise, continuously disturbing the rotating disk boundary layer. As conjectured by Pier [32], this flow region could be locally absolutely unstable, triggering a global mode, that cannot be suppressed, at $Re_\delta < Re_{\delta_{ca}}$ (see Fig.5 in Ref. [44] where $Re_{\delta_{ca}}$ is estimated from the local stability analysis of the mean flow). This global front would be edge-driven since depending on the conditions at the edge and moving upstream when the rotation is increased as shown on on Fig.10. Note that this feature is not documented in the work of Makino *et al.* [76], and it is unclear whether this region has not been studied by the authors or whether the boundary conditions used do not lead to the same behaviour.

At higher rotation rates, the front is now located at the convective/absolute transition location predicted by the local linear stability analysis and its characteristics are no longer dependent of the Reynolds number at the edge. As a consequence, it may be considered as a self-sustained rotor boundary layer global mode resulting from the superposition of several absolutely unstable modes. A secondary front related to a secondary instability is also conspicuously close to $Re_\delta = 538$ and immediately followed by incipient turbulence, similar to the *absolute* scenario in the clean single-disk. This scenario seems similar to the one observed in the angular sector of an open rotating disk cavity with radial throughflow by Viaud *et al.* [43], where the inflow boundary conditions have been specifically designed to limit undesired self-sustained perturbations. Indeed, Viaud *et al.* showed that the rotating disk boundary layer is globally linearly stable and globally non-linearly unstable. The transition is thus governed by a non-linear

global mode, characterized by a front of spiral arms located at the convective/absolute instability transition, and immediately followed by a secondary front ($Re_\delta = 538$) and incipient turbulence.

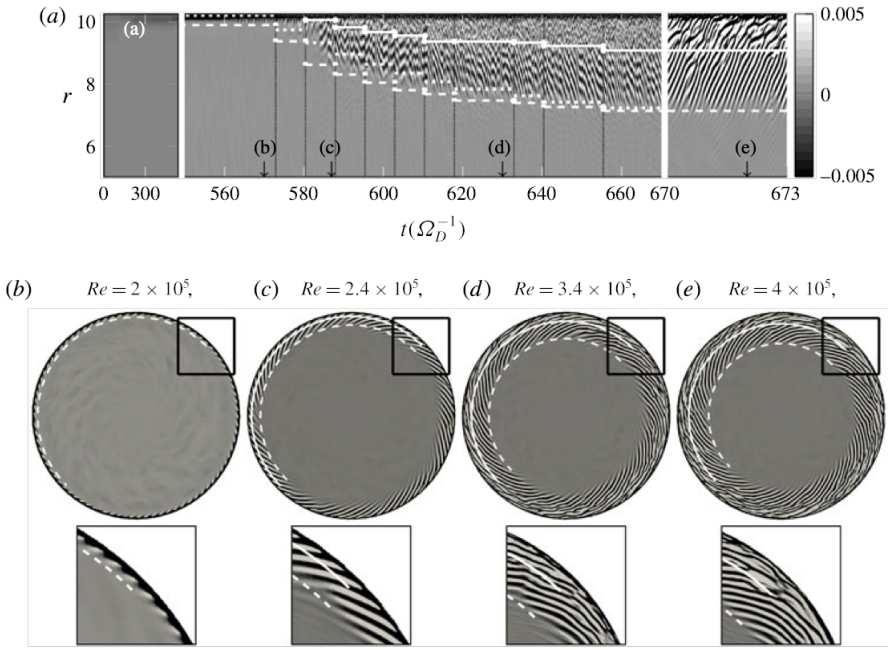

Figure 10: Temporal evolution of the flow patterns in the rotor boundary layer of the cylindrical rotor-stator cavity when increasing Reynolds number in the range $Re \in [2 \times 10^5, 4 \times 10^5]$, a copy of Figure 4 of Ref. [44]. (a) Spatio-temporal diagram. (b–e) Instantaneous top views of axial velocity field w corresponding to four Re, at time instants as indicated on (a). The white dashed (– – –) and solid (——) lines in (a–e) show the positions of the primary and secondary fronts, respectively. The white dotted line (· · ·) in (a) is $r = Re_\delta^{c/a} \Gamma / \sqrt{Re \Omega \Omega_d^{-1}}$ with $Re_\delta^{c/a} = 425$ from table 1 in [38].

6. Concluding remarks

This article aims at reviewing the main results of the literature related to the instabilities and routes to turbulence over rotating single-disks and in rotating cavities, with two generic configurations for this latter: the rotor-stator cavity and the open co-rotating cavity with radial throughflow. Although research on this subject is almost one hundred years old, the abundant literature published over the last ten years shows that it is still active today and continues to unveil original results. The works collected in this paper show the links that exist between the boundary layer over a rotating single-disk and the flows that develop near the disks in rotating cavities, both in terms of base flows and instability mechanisms and routes to turbulence that seem to emerge in the most recent studies. However, the cavities show some specificities mainly due to the flow confinement in both radial and axial directions, which can modifies locally the boundary-layer base flow as well as the transition to turbulence by introducing some feedback mechanisms between the boundary layers.

The abundance of different flow features and transition scenarios in these configurations may boil down to the competition between the stabilising radial inhomogeneity of the base flow and

the non-linear destabilisation of the perturbations, i.e. a competition between linear and non-linear mechanisms on one hand and local and global stability properties on the other hand. Within this framework, the rotating-disk boundary layer can be found to be simultaneously locally absolutely unstable, globally linearly stable and globally non-linearly unstable. The discrepancy observed between the global linear and non-linear dynamics is mainly due to the existence of large convectively unstable region upstream of the absolutely unstable region. Then, it is very difficult to eliminate stationary cross-flow vortices in experiments excited by the unavoidable surface roughness of the disks whose the characteristics (size, shape, distribution, ...) determine the route to turbulence. In this context, computing the main receptivity characteristics of the rotating disk boundary layer to surface roughness becomes necessary for predicting the possible routes to turbulence as shown in the recent work of Thomas and Davies based on adjoint approach.

The review shows that the progress made in recent years in fully non-linear direct numerical simulations make them reliable to investigate transition to turbulence, in well-controlled numerical experiments facilitating the confrontation with theory and allowing a better and easier interpretation of experimental measurements.

The most recent papers focus on the routes to turbulence. To date, the complete process of transition has yet to be fully characterised but nevertheless the scenarios can be classified as convective or absolute depending on how the primary instability is triggered. Both are based on the existence of an absolutely unstable zone of sufficient radial extent, the former requires external forcing while the latter is self-sustained.

As mentioned in the paper these scenarios imply a secondary instability that remains poorly documented in the current literature, preventing any conclusive results on the final stages of the transition. Some reasons could be the high Reynolds numbers involved requiring high resolution and costly computations, the weak amplitude of the phenomenon with respect to the primary instability and finally the fast transition to turbulence once it appears. It was observed experimentally many years ago just before the turbulent breakdown region and associated to high frequencies [68,79,80]. However, the first attempt to provide reliable results on secondary instability was certainly the pioneering theoretical work of Pier [55] which showed that the primary saturated waves initiated by the front at $Re_\delta^{c/a}$ are already absolutely unstable with respect to these secondary perturbations. Thus, due to secondary absolute instability, this naturally selected primary structure is dynamically unstable and immediately gives way to turbulence. Numerically and experimentally this secondary instability has been associated both in the single-disk and in the cavity configurations to a secondary front occurring downstream of the first one. It is characterized by a region of exponential growth where the spectrum fills out (which could indicate absolute instability of the saturated primary instability to secondary instabilities leading directly to turbulence) [43]. It is characterized by a change in slope of the vrms profiles and the appearance of skewness [33](Imayama expe 2013). to the rapid growth of the high-frequency components in the spectra shown in figure5a (Imayama 2014).

(single disk Imayama 2013; Appelquist et al. 2016, cavity (Viaud et al. 2011; Yim 2018. The difference between the results of Viaud et al. (2011) and Pier (2003) is largely that the latter found that the secondary instability with largest absolute growth rate is a subharmonic mode whereas Viaud et al.'s (2011) secondary instability is not subharmonic.

Unfortunately measurements made by Imayama 2013 using a single hot-wire probe fixed in the laboratory frame cannot easily capture the characteristics of the travelling secondary instabilities such as the frequency and growth rate. Further research would be required to characterize these instabilities fully.

For [63] [71]???? secondary global instability is triggered by the flow at the disk edge. For Makino: smaller-scale structures, perhaps resulting from the secondary instability, appear outside the primary patterns. Note that inflection points tend to appear in the instantaneous velocity

profiles, particularly in the low-speed regions (see the circles in Fig.13). According to the Rayleigh theorem, this type of velocity profile is known to produce a secondary instability wave. Thus, it is said that the secondary instability occurs due to the interaction between the dominant S-C instability and the main flow. A similar scenario has been reported for a disturbed boundary-layer on a single rotating disk by Faller (1991).

To describe the precise transition scenario an extensive investigation of secondary instabilities is needed, and further simulations are planned to investigate the interactions between the various instability modes

The conclusion text goes here.

RECEPTIVITY ??????????????????????????????????????There is only

Ethics. Insert ethics statement here if applicable.

Data Accessibility. Insert details of how to access any supporting data here.

Authors' Contributions. For manuscripts with two or more authors, insert details of the authors' contributions here. This should take the form: 'AB caried out the experiments. CD performed the data analysis. EF conceived of and designed the study, and drafted the manuscript All auhtors read and approved the manuscript'.

Competing Interests. Insert any competing interests here. If you have no competing interests please state 'The author(s) declare that they have no competing interests'.

Funding. Insert funding text here.

Acknowledgements. Insert acknowledgment text here.

Disclaimer. Insert disclaimer text here if applicable.

Bibliography

References

1. G. I. Taylor.
Stability of a viscous liquid contained between two rotating cylinders.
Phil. Trans. of the Royal Society of London. Series A, 223:289 – 343, 1923.
2. O. Czarny, E. Serre, P. Bontoux, and R. M. Lueptow.
Interaction between the ekman pumping and the centrifugal instability in taylor-couette flow.
Phys. Fluids, 15(2):467 – 477, 2003.
3. O. Czarny, E. Serre, P. Bontoux, and R. M. Lueptow.
Interaction of wavy cylindrical couette flow with endwalls.
Phys. Fluids, 16(4):1140–1148, 2004.
4. J. M. Owen and R. H. Rogers.
Flow and Heat Transfer in Rotating-Disc Systems, Volume 1: Rotor-Stator Systems.
Wiley, 1989.
5. J. M. Owen and R. H. Rogers.
Flow and Heat Transfer in Rotating-Disc Systems. Volume 2: Rotating Cavities.
Wiley, 1995.
6. E. Crespo del Arco, E. Serre, P. Bontoux, and B. E. Launder.
Stability, transition and turbulence in rotating cavities.
In M. RAHMAN, editor, *Advances in Fluid Mechanics*, volume 41 of *Dalhousie University Canada Series*, pages 141–196. WIT press, 2005.
7. B. E. Launder, S. Poncet, and E. Serre.
Transition and turbulence in rotor-stator flows.
Ann. Rev. Fluid Mech., 42:229 – 248, 2010.
8. R. Hide.
On source-sink flows stratified in a rotating annulus.
J. Fluid Mech., 32:737–764, 1968.
9. H. P. Greenspan.
The theory of rotating fluids.

Cambridge University Press, 1968.
10. L. Schouveiler, P. Le Gal, and M.-P. Chauve.
Instabilities of the flow between a rotating and a stationary disk.
J. Fluid Mech., 443:329–350, 2001.
11. A. Cros and P. Le Gal.
Spatiotemporal intermittency in the torsional couette flow between a rotating and a stationary disk.
Phys. Fluids, 14:3755–3765, 2002.
12. Th. von Kármán.
Über laminare und turbulente Reibung.
Z. Angew. Math. Mech, 1:233–252, 1921.
13. R. J. Lingwood and H. P. Alfredsson.
Instabilities of the von kármán boundary layer.
Applied Mechanics Reviews, 67(3):030803–1 – 030803–13, 2015.
14. N. H. Smith.
Exploratory investigation of boundary layer oscillations on a rotating disc.
NACA Tech. Note, 1227, 1947.
15. N. Gregory, J. T. Stuart, and W. S. Walker.
On the stability of three-dimensional boundary layers with applications to the flow due to a rotating disk.
Phil. Trans R. Soc. London, 248:155–199, 1955.
16. D. K. Lilly.
On the instability of the Ekman layer flow.
J. Atmos. Sc., 23:481–494, 1966.
17. A. J. Faller.
An experimental study of the instability of the laminar ekman boundary layer.
J. Fluid Mech., 15:560–576, 1963.
18. P. R. Tatro and E. Mollo-Christensen.
Experiments on Ekman layer instability.
J. Fluid Mech., 28:531–544, 1967.
19. A. J. Faller and R. Kaylor.
Instability of the ekman spiral with applications to the planetary boundary layers.
Phys. Fluid, 10:S212–, 1967.
20. A. J. Faller.
Instability and transition of a disturbed flow over a rotating disk.
J. Fluid Mech., 230:245–269, 1991.
21. R. J. Lingwood.
Absolute instability of the boundary layer on a rotating disk.
J. Fluid Mech., 299:17–33, 1995.
22. R. J. Lingwood.
An experimental study of the absolute instability of the rotating-disk boundary-layer flow.
J. Fluid Mech., 314:373–405, 1996.
23. R. J. Lingwood.
Absolute instability of the Ekman layer and related rotating flows.
J. Fluid Mech., 331:405–428, 1997.
24. R. J. Lingwood.
On the effects of suction and injection on the absolute instability of the rotating disk boundary layer.
Phys. Fluid, 9:1317–1328, 1997.
25. C. Thomas and C. Davies.
An adjoint approach for computing the receptivity of the rotating disc boundary layer to surface roughness.
J. Fluid Mech., 926:A16, 2021.
26. S. Imayama, P. H. Alfredsson, and R. J. Lingwood.
Experimental study of rotating-disk boundary-layer flow with surface roughness.
J. Fluid Mech., 786:5–28, 2016.
27. C. Davies and P. W. Carpenter.
Global behaviour corresponding to the absolute instability of the rotating-disk boundary layer.

J. Fluid Mech., 486:287–329, 2003.
28. C. Davies, C. Thomas, and P. W. Carpenter.
Global stability of the rotating-disk boundary layer.
J. Eng. Math., 57:219–236, 2007.
29. H. Othman and T. C. Corke.
Experimental investigation of absolute instability of a rotating-disk boundary layer.
J. Fluid Mech., 565:63–94, 2006.
30. J.J. Healey.
Enhancing the absolute instability of a boundary layer by adding a far-away plate.
J. Fluid Mech., 579:29–61, 2007.
31. E. Appelquist, P. Schlatter, P. H. Alfredsson, and R. J. Lingwood.
On the global nonlinear instability of the rotating-disk flow over a finite domain.
J. Fluid Mech., 803:332–355, 2016.
32. B. Pier.
Transition near the edge of a rotating disk.
J. Fluid Mech., 737, 2013.
33. S. Imayama, P. H. Alfredsson, and R. J. Lingwood.
An experimental study of edge effects on rotating-disk transition.
J. Fluid Mech., 716:638–657, 2007.
34. G. K. Batchelor.
Note on a class of solutions of the navier–stokes equations representing steady rotationally-symmetric flow.
Quat. J. Mech. and Appl. Math., 4:29–41, 1951.
35. G. K. Batchelor.
The theory of homogeneous turbulence.
Cambridge University Press, 1953.
36. P. J. Zandbergen and D. Dijkstra.
Vonkármán swirling flows.
Ann. Rev. Fluid Mech., 19:465–491, 1986.
37. N. Itoh.
On the stability of flow between coaxial rotating disks.
ASME Boundary layer stability and transition to turbulence, 114, 1991.
38. E. Serre, E. Tuliszka-Sznitko, and P. Bontoux.
Coupled numerical and theoretical study of the flow transition between a rotating and a stationary disk.
Phys. Fluids, 16:688–706, 2004.
39. D. Dijkstra and G. J. F. van Heijst.
The flow between two finite rotating discs enclosed by a cylinder.
J. Fluid Mech., 128:123, 1983.
40. J. F. Brady and L. Durlofsky.
On rotating disk flow.
J. Fluid Mech., 175:363–394, 1987.
41. J. M. Lopez.
Characteristics of endwall and sidewall boundary layers in a rotating cylinder with a differentially rotating endwall.
J. Fluid Mech., 359:49–79, 1998.
42. R. Corral and D. Romera.
On the transient behaviour of a laminar rotor–stator cavity.
J. Fluid Mech., 857:508–538, 2018.
43. B. Viaud, E. Serre, and J.-M. Chomaz.
Transition to turbulence through steep global-mode cascade in an open rotating cavity.
J. Fluid Mech., 688:493–506, 2011.
44. E. Yim, J.-M. Chomaz, D. Martinand, and E. Serre.
Transition to turbulence in the rotating disk boundary layer of a rotor–stator cavity.
J. Fluid Mech., 848:631–647, 2018.
45. E. Serre, S. Hugues, E. Crespo del Arco, A. Randriamampianina, and P. Bontoux.
Axisymmetric and three-dimensional instabilities in an Ekman boundary-layer flow.
Int. J. Heat Fluid Flow, 22:82–93, 2001.

46. J. M. Lopez and F. Marques.
Sidewall boundary layer instabilities in a rapidly rotating cylinder driven by a differentially corotating lid.
Phys. of Fluids, 22:114109, 2010.
47. E. Crespo del Arco, P. Maubert, A. Randriamampianina, and P. Bontoux.
Spatio-temporal behaviour in a rotating annulus with a source-sink flow.
J. Fluid Mech., 32:1–27, 1996.
48. P. R. N. Childs.
Rotating flows.
Elsevier, 2011.
49. V. W. Ekman.
On the influence of earth's rotation on ocean currents.
Arkiv. Math. Astr .Fys, 2(11):1–52, 1905.
50. U. T. Bödewadt.
Die Drehströmung über festem Grunde.
Z. Angew. Math. Mech, 20:241–253, 1940.
51. N. Cousin-Rittemard, O. Daube, and P. Le Quéré.
Structuration de la solution stationnaire des écoulements interdisques en configuration rotor–stator.
C. Acad. Sciences Série IIb, 6:221–226, 1999.
52. B. Viaud, E. Serre, and J.-M. Chomaz.
The elephant mode between two rotating disks.
J. Fluid Mech., 598:451–464, 2008.
53. G. Gauthier, P. Gondret, and M. Rabaud.
Axisymmetric propagating vortices in the flow between a stationary and a rotating disk enclosed by a cylinder.
J. Fluid Mech., 386:105–126, 1998.
54. L. M. Mack.
The wave pattern produced by a point source on a rotating-disk flow.
AIAA paper, 85-0490, 1985.
55. B. Pier.
Finite amplitude crossflow vortices, secondary instability and transition in the rotating-disk boundary layer.
J. Fluid Mech., 487:315–343, 2003.
56. S. P. Wilkinson and M. R. Malik.
Stability experiments in rotating disk flows.
AIAA J., 83:560–576, 1983.
57. M. Turkyilmazoglu and J. S. B. Gajjar.
Direct spatial resonnance in the laminar boundary layer due to a rotating disk.
Sadhana - Acad. Proc., 25:601–617, 2000.
58. S. Takagi and N. Itoh.
The mode selection mechanism of cross-flow instability in three-dimensional boundary layers.
Technical report, JAXA, 2004.
59. N. Itoh.
Simple cases of streamline-curvature instability in three-dimensional boundary layers.
J. Fluid Mech., 317:129–154, 1996.
60. P. Huerre and P. A. Monkewitz.
Absolute and convective instabilities in free shear layers.
J. Fluid Mech., 159:151–168, 1985.
61. E. Appelquist, P. Schlatter, P. H. Alfredsson, and R. J. Lingwood.
Global linear instability of the rotating-disk flow investigated through simulations.
J. Fluid Mech., 765:612–631, 2015.
62. A. Couairon and J.-M. Chomaz.
Absolute and convective instabilities, front velocities and global modes in nonlinear systems.
Physica D, 108:236–276, 1997.
63. E. Appelquist, P. Schlatter, P. H. Alfredsson, and R. J. Lingwood.
Transition to turbulence in the rotating-disk boundary-layer flow with stationary vortices.
J. Fluid Mech., 836:43–71, 2018.

64. J. J. Healey.
Model for unstable global modes in the rotating-disk boundary layer.
J. Fluid Mech., 663:148–159, 2010.
65. B. Pier.
Open-loop control of absolutely unstable domains.
Proc. R. Soc. Lond. A, 459:1105—1115, 2003.
66. K. Lee, Y. Nishio, S. Izawa, and Y. Fukunishi.
The effect of downstream turbulent region on the spiral vortex structures of a rotating-disk flow.
J. Fluid Mech., 844:274–296, 2018.
67. B. Pier.
Primary crossflow vortices, secondary absolute instabilities and their control in the rotating-disk boundary layer.
J. Eng. Math., 57:237–251, 2007.
68. R. Kobayashi, Y. Kohama, and C. Takadamate.
Spiral vortices in boundary transition regime on a rotating disk.
Acta Mech., 35:79–82, 1980.
69. M. R. Malik, S. P. Wilkinson, and S. A. Orszag.
Instability and transition in rotating disk flow.
AIAA J., 19:1131–1138, 1981.
70. C. Thomas and C. Davies.
On the impulse response and global instability development of the infinite rotating-disc boundary layer.
J. Fluid Mech., 857:239–269, 2018.
71. S. Imayama, P. H. Alfredsson, and R. J. Lingwood.
On the laminar-turbulent transition of the rotating-disk flow: the role of absolute instability.
J. Fluid Mech., 745:132–163, 2014.
72. S. Imayama, P. H. Alfredsson, and R. J. Lingwood.
A new way to describe the transition characteristics of a rotating-disk boundary-layer flow.
Phys. Fluids, 24:031701, 2012.
73. E. Severac and E. Serre.
A spectral vanishing viscosity for the les of turbulent flows within rotating cavities.
J. Comput. Phys., 226:1234–1255, 2007.
74. E. Severac, S. Poncet, E. Serre, and M. P. Chauve.
Large eddy simulation and measurements of turbulent enclosed rotor-stator flows.
Phys. of Fluids, 19(8):085113, 2007.
75. F. Gao and J. W. Chew.
Evaluation and application of advanced cfd models for rotating disc flows.
J. Mechanical Engineering Science, 235(23):6847–6864, 2021.
76. S. Makino, M. Inagaki, and M. Nakagawa.
Laminar-turbulence transition over the rotor disk in an enclosed rotor-stator cavity.
Flow Turb. Comb., 95:399–423, 2015.
77. S. Poncet, M. P. Chauve, and P. Le Gal.
Turbulent rotating disk flow with inward throughflow.
J. Fluid Mech., 522:253–262, 2004.
78. A. Cros, F. Floriani, P. Le Gal, and R. Lima.
Transition to turbulence of the batchelor flow in a rotor/stator device.
Eur. J. Mech. (B/Fluids), 24:409–424, 2005.
79. S. P. Wilkinson and M. R. Malik.
Stability experiments in the flow over a rotating disk.
AIAA J., 23:588—595, 1983.
80. Y. Kohama.
Study on boundary layer transition of a rotating disk.
Acta Mechanica, 50:193–199, 1984.